The interplay between the Aharonov-Bohm interference and parity selective tunneling in graphene nanoribbon rings

2014 J. Phys.: Condens. Matter 26 205301

(http://iopscience.iop.org/0953-8984/26/20/205301)

IOP Publishing Journal of Physics: Condensed Matter
J. Phys.: Condens. Matter **26** (2014) 205301 (8pp) doi:10.1088/0953-8984/26/20/205301

The interplay between the Aharonov-Bohm interference and parity selective tunneling in graphene nanoribbon rings

V Hung Nguyen[1,2], Y-M Niquet[1] and P Dollfus[3]

[1] L_Sim, SP2M, UMR-E CEA/UJF-Grenoble 1, INAC, 38054 Grenoble, France
[2] Center for Computational Physics, Institute of Physics, Vietnam Academy of Science and Technology, PO Box 429 Bo Ho, 10000 Hanoi, Vietnam
[3] Institute of Fundamental Electronics (IEF), UMR8622, CNRS, Univ. Paris Sud, 91405 Orsay, France

E-mail: hung@iop.vast.ac.vn

Received 11 December 2013, revised 19 March 2014
Accepted for publication 21 March 2014
Published 1 May 2014

Abstract

We report on a numerical study of the Aharonov–Bohm (AB) effect and parity selective tunneling in *pn* junctions based on rectangular graphene rings where the contacts and ring arms are all made of zigzag nanoribbons. We find that when applying a magnetic field to the ring, the AB interference can reverse the parity symmetry of incoming waves and hence can strongly modulate the parity selective transmission through the system. Therefore, the transmission between two states of different parity exhibits the AB oscillations with a π–phase shift, compared to the case of states of the same parity. On this basis, it is shown that interesting effects, such as giant (both positive and negative) magnetoresistance and strong negative differential conductance, can be achieved in this structure. Our study thus presents a new property of the AB interference in graphene nanorings, which could be helpful for further understanding the transport properties of graphene mesoscopic systems.

Keywords: graphene nanoribbon ring, Aharonov–Bohm effect, tunneling, Green's function

(Some figures may appear in colour only in the online journal)

The Aharonov–Bohm (AB) interference [1] is an elegant way of investigating phase coherent transport in mesoscopic systems. When a perpendicular magnetic field B is applied to a ring connected to two leads, the transmission probability exhibits oscillations with a characteristic period $\Delta B = \phi_0/S$ as a consequence of a phase difference $\Delta\phi = 2\pi\, BS/\phi_0$ between the two arms forming the ring. Here, S is the area of the ring and $\phi_0 = h/e$. The AB oscillations have been intensively studied and were observed in several systems such as metal rings [2], semiconductor heterostructures [3], carbon nanotubes [4, 5], topological insulators [6] and recently in graphene rings (see the review [7]).

Due to its amazing electronic properties, graphene has recently become a material of particular interest (e.g. see the review [8]). Numerous unusual transport phenomena, such as finite minimal conductivity, Klein tunneling, chiral properties of charge carriers and unconventional quantum Hall effects, have been explored in graphene nanostructures. With a specific electronic band structure, graphene has another remarkable property: the charge carriers in both conduction and valence bands can be involved simultaneously in the transport, as for instance in Klein tunneling [9] and band-to-band tunneling regimes [10]. This property has motivated studies on the AB effect in electron–hole graphene rings [11–13], where a gate voltage was applied locally to one of two ring arms so as to generate interferences between electron–electron, hole–hole and electron–hole states. These studies allowed for an understanding of the interplay between the AB effect and Klein tunneling, both away from and at the Dirac (charge neutrality) point. Additionally, they demonstrated AB interference, regardless of the charge carrier type in the ring arms [13].

Besides the phenomena mentioned above, it has been shown that lattice symmetry is also a peculiar property of graphene nanoribbons (GNRs). For instance, theoretical

works have predicted that one-third of armchair edge GNRs are semimetals with a negligible band gap and the rest are semiconductors, while zigzag GNRs present spin polarized edges and edge localized states (see in [8]). In the zigzag GNR structures, some studies [14–18] have additionally predicted a phenomenon called the parity selective rule, which implies that the transmission between different subbands strongly depends on their even–odd parity. This phenomenon leads to interesting features such as negative differential conductance (NDC) behavior, the valley-valve effect and the band selective filter. In a recent work [19], we have demonstrated that strong AB oscillations can be achieved in rectangular GNR rings in the energy regime where only a single band is active. However, another interesting issue, the interplay between the AB interference and parity selective tunneling, has not been studied yet. In this article, we investigate the magnetotransport in *pn* junctions based on zigzag GNR rings, as schematized in figure 1, where both effects can be observed simultaneously if the contact GNRs have an even number of zigzag lines. We will show that the parity selective rule can be modulated by AB interference. In particular, the AB effect can reverse the parity symmetry of incoming waves, so that the transmission between states of different parity is significantly enhanced. We have found a new property: compared to the case of same parity, there is a π–phase shift of AB oscillations when incoming and outgoing states have different parities. On this basis, strong AB oscillations with giant positive (negative) magnetoresistance at low (high) bias and strong NDC behavior can be achieved, even at room temperature.

The transport properties of the GNR ring (see in figure 1) under a perpendicular magnetic field (B–field) are investigated using the Green's function method [20] to solve a nearest-neighbor tight-binding model, as in [19]. The presence of the B–field is included using the Peierls phase approximation [21]. The hopping integral between nearest-neighbor atoms is hence given by $t_{\rm nm} = -\tau_0 \exp(\mathrm{i}\phi_{\rm nm})$, where $\tau_0 \approx 2.7$ eV [22] and $\phi_{\rm nm} = \dfrac{2\pi}{\phi_0}\int_{\mathbf{r}_n}^{\mathbf{r}_m} \mathbf{A}(\mathbf{r})\,\mathrm{d}\mathbf{r}$. The vector potential $\mathbf{A}(\mathbf{r}) = (-By, 0, 0)$ is related to the magnetic field $\mathbf{B} = (0, 0, B)$ by $\nabla \times \mathbf{A} = \mathbf{B}$. The considered ring is characterized by the set of parameters of figure 1. The width of the GNRs (i.e. the numbers of zigzag lines $Q_{\rm c}$, $Q_{\rm r}$, $Q_{\rm h}$) is given in units of $3a_{\rm c}/2$, their length ($N_{\rm h}$, $N_{\rm s}$) is given in units of $a_{\rm c}\sqrt{3}$ with $a_{\rm c} = 1.42$ Åand the difference between the potential energies in p-doped and n-doped zones is U_0. Within the Green's function framework, the transmission probability needed to evaluate the current and the local density of states (LDOS) are calculated as $\mathcal{T}(\varepsilon, B) = Tr[\Gamma_L G^r \Gamma_R G^{r\dagger}]$ and $D(\varepsilon, B; \mathbf{r}_n) = -\mathrm{Im}\left\{G^r_{n,n}(\varepsilon, B)\right\}/\pi$, respectively, from the device-retarded Green's function $G^r(\varepsilon, B)$, the injection rate $\Gamma_{L(R)} = \mathrm{i}(\Sigma_L - \Sigma_L^\dagger)$ and the self-energy $\Sigma_{L(R)}$ defining the left (right) contact-to-device coupling. The current $\mathcal{I}(B)$ is computed using the Landauer formula [19] and the magnetoresistance (MR) is finally defined as $MR = [\mathcal{I}(B) - \mathcal{I}(0)]/\mathcal{I}(B)$.

It has been shown in the literature that due to their lattice symmetry, each subband of zigzag GNRs has a parity characterizing the even-odd property of its wave function under a mirror reflection [14–18]. This property leads to a parity selective rule on the transmission (i.e. parity selective tunneling mentioned above) through the GNRs having an even number of zigzag lines. In particular, the transmission between two states of different parity (e.g. as indicated in figure 1) is forbidden, while it is possible between states of the same parity. We now investigate the AB interference for different parity properties of charge carriers. In figure 2, we display the transmission probability as a function of energy at different B–fields in a uniform zigzag GNR *pn* junction and *pn* junctions based on zigzag GNR rings. In all these cases, $Q_{\rm c}$ is even, so that the parity selective tunneling manifests very well in the transport picture, i.e. at $B = 0$ a clear energy gap occurs consistently with the fact that the two states have a different parity while the ring is transparent beyond this gap.

First, let us introduce briefly the principle of this tunneling rule in the *pn* junctions based on uniform zigzag GNRs. Based on the analysis in [17], any crystalline wave function in the GNR made of Q zigzag carbon chains can be expressed as a linear combination of Bloch sums

$$\Psi(\mathbf{k}, \mathbf{r}) = \sum_{j=1}^{Q} \alpha_j \Phi_j(\mathbf{k}, \mathbf{r}) + \alpha_{2Q+1-j}\Phi_{2Q+1-j}(\mathbf{k}, \mathbf{r}) \,, \quad (1)$$

where $\Phi_j(\mathbf{k}, \mathbf{r})$ is built from the $2Q$ orbitals in the primitive cell (see equation (3) of [17]) and $\mathbf{k}$ is the one-dimensional wave vector. In this equation, the first (second) term is the lower (upper) part of the wave function, while the coefficients α_j satisfy the relation $\alpha_{2Q+1-j} = \pm\alpha_j$ depending on its even/odd parity, which essentially arises from the crystal symmetry of zigzag GNRs. The parity symmetry of each subband in two different GNR classes of even/odd number Q has been shown in figures 5(a) and (b) of [17]. The transmission process illustrated in figure 1 was demonstrated to be possible only if the superimposed potential $U(x)$ acts as an intervalley scattering source [16, 17]. It was then shown in [17] that the matrix element $U_{\alpha\beta}$ of U between two states $\Psi_\alpha(\mathbf{k})$ and $\Psi_\beta(\mathbf{q})$ of different parity is zero in the GNRs of even number Q; the transmission is hence blocked. Otherwise, $U_{\alpha\beta}$ is generally nonzero and the transmission is opened in the case of same parity or in the GNRs of odd Q. These features were named the parity selective tunneling [14] and essentially explain the data of figure 2(*a*). The presence of a B–field, in principle, modifies the relation above between α_{2Q+1-j} and α_j, so that the analysis above becomes no longer completely valid, i.e. the transmission probability in the gap region slightly increases when increasing the B–field (see the inset of figure 2(*a*)). However, in the range of B–field studied in this work, this effect is negligible, compared to the AB interference, as discussed below.

We now analyze the transport properties of *pn* junctions based on zigzag GNR rings. At $B = 0$, the results displayed in figures 2(*b*) and (*c*) show that, compared to the uniform GNR *np* junction, the presence of the GNR ring does not affect the energy gap but results in resonant effects outside this gap. However, these resonant effects are not strong in these zigzag GNR rings, as compared to that observed in armchair ones, as discussed in [19]. Basically, the achievement of an unchanged energy gap suggests that the parity selective

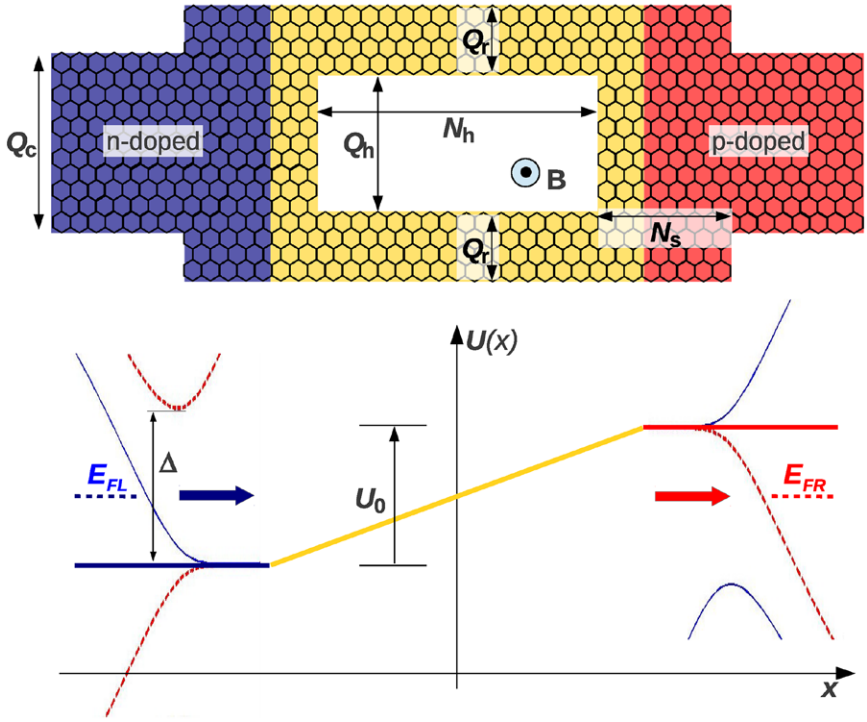

Figure 1. Schematic of the graphene nanoribbon ring considered in this work and its energy band profile. Q_r, Q_c and Q_h characterize the width of the ring, of the contact graphene nanoribbons and of the hole, respectively. N_h defines the length of the hole and N_s stands for the size of side nanoribbons along the transport direction. U_0 is the potential difference between p-doped and n-doped zones, while $E_{FL(R)}$ denotes the Fermi level in the left (right) contact.

rule is still valid in these considered heterostructures. When increasing the B–field, we find an interesting feature that the AB effect can change the parity selective tunneling, i.e. the transmission probability can be significantly enhanced in the gap regime. Moreover, the AB oscillations of the transmission between two states of different parity in the gap regime (II) have a π–phase shift when compared to the case of same parity in the regimes (I) and (III), which will be shown more clearly by the B–dependence of the current later. A π–phase shift of the AB oscillations has also been observed in side-gated graphene rings [23] by changing the gate voltages, which is explained by the generalized Onsager symmetry that is essentially different from the phenomenon observed here, as will be discussed below. Note that, due to the contribution of several subbands to the transport [19], the AB effect is weak beyond the energy regimes (I–III). We also distinguish two different cases depending on the even or odd number Q_r of the GNRs in the ring arms. The transmission exhibits strong oscillations in the whole gap region if Q_r is odd (figure 2(*c*)). If Q_r is even (figure 2(*b*)), these strong oscillations are simply limited to the energies close to the potential energy in the n-doped and p-doped zones. However, in this case of even Q_r, we have found, as shown in figure 2(*b*), that if the ring is totally placed in the zone of a unique doping type (i.e. *n*-doped or *p*-doped), the transmission can be significantly modulated in almost the whole gap region, similarly to the case of odd Q_r.

These results can be explained as follows. When entering the ring, the trajectories of charge carriers are spatially separated in the upper and lower ring arms and the wave function in the ring is hence described by two separate parts, respectively. At zero B–field, these two parts still preserve the parity symmetry supported by the GNR contact when crossing the ring arms, because of the symmetry of the two studied arms. This explains why the parity selective rule is still valid in the considered rings at $B = 0$. However, in the presence of a finite B–field these two parts of the incoming wave are subject to two different phase shifts [1], i.e. the upper (lower) part is multiplied by a phase prefactor $\exp\left(-\mathrm{i}\frac{\phi(B)}{2}\right)\left(\exp\left(\mathrm{i}\frac{\phi(B)}{2}\right)\right)$ with $\phi(B) = 2\pi BS/\phi_0$. Note that this phase difference is essentially determined by the magnetic flux applied to the ring and S is the area of the surface enclosed by the trajectories of charge carriers in the two ring arms. For instance, if the B-field is artificially applied on a surface limited to the inner hole, S is simply the area of this surface. In our case where the B-field is applied to the whole ring, the magnetic flux characterizing the AB oscillations is determined with the average area of inner and outer surfaces of the ring. In particular, $S \approx 258$ nm^2 and the period of AB oscillations $\Delta B = \phi_0/S \approx 16$ T here. These phase prefactors satisfy $\exp\left(\mathrm{i}\frac{\phi(B)}{2}\right) = \exp\left(-\mathrm{i}\frac{\phi(B)}{2}\right) = (-1)^n$ if $B = n\phi_0/S$ while $\exp\left(\mathrm{i}\frac{\phi(B)}{2}\right) = -\exp\left(-\mathrm{i}\frac{\phi(B)}{2}\right) = (-1)^n\,\mathrm{i}$ when $B = (n+½)\,\phi_0/S$. The appearance of these phase prefactors and their B–dependence are basically responsive for the AB oscillations in all cases [1].

We now distinguish two different cases studied in this work. First, if the parity selective rule does not apply, the ring is generally transparent at $B = n\phi_0/S$, while the transmission is blocked when $B = (n+½)\,\phi_0/S$. This explains

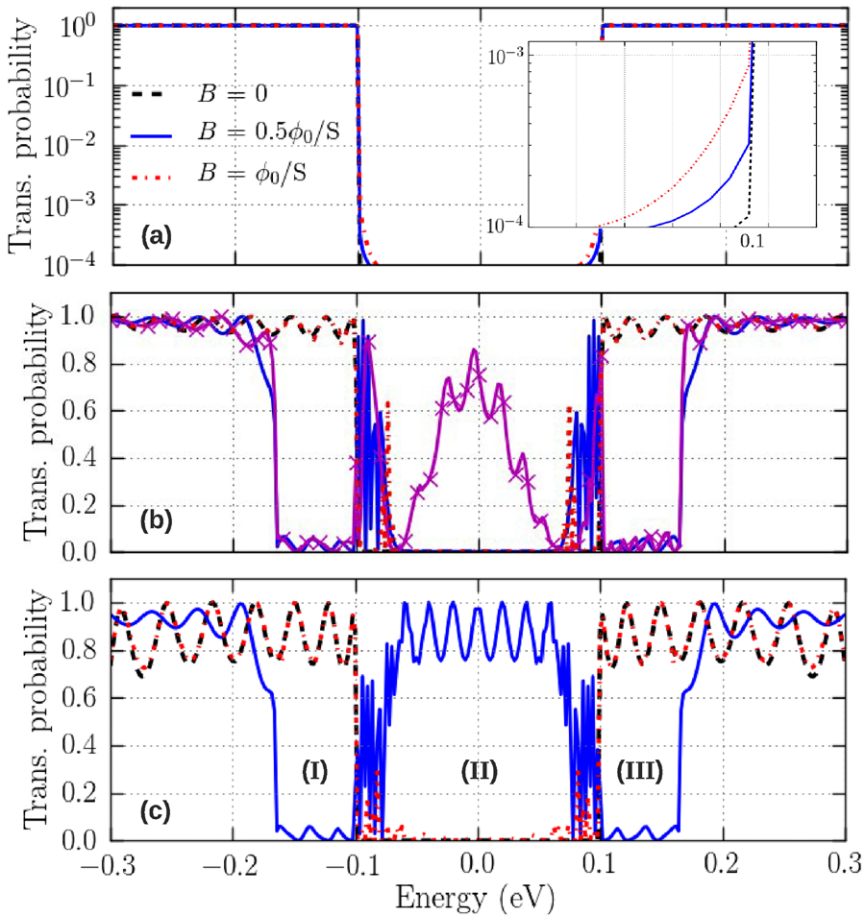

Figure 2. Transmission probability as a function of energy at different B−fields: (*a*) uniform zigzag GNR *pn* junction and (*b*, *c*) *pn* junctions based on zigzag GNR rings with even (= 22) and odd Q_r (= 21), respectively. The inset in (*a*) shows a zoomed image of the transmission probability around $E = 0.1$ eV. The × solid curve in (*b*) shows the data obtained at $B = 0.5 \times \phi_0/S$ in the GNR ring of $Q_r = 22$ where the whole ring is displaced to the *p*-doped zone. In (*c*) the energy regions (I), (II) and (III) distinguish different transport regimes. $Q_c = 46$ everywhere and other parameters are $U_0 = 0.2$ eV, $Q_h = 14$ in (*b*) and 16 in (*c*), $N_h = 120$ and $N_s = 11$ in (*b*, *c*).

not only the AB oscillations observed for the transmission between states of the same parity (i.e. see the energy regimes (I) and (III) in figure 2) in the rings considered here, but also the AB oscillations observed in other systems such as the armchair GNR rings [19] and the zigzag GNR rings with the GNR contacts of odd number Q_c. In contrast, if the parity selective rule applies, since the two phase prefactors are identical when $B = n\phi_0/S$, the parity symmetry is still preserved as at $B = 0$ and the transmission between two states of different parity is hence forbidden. When $B = (n + ½)\,\phi_0/S$, the two phase prefactors have opposite signs, so that the parity symmetry of the incoming wave is reversed when crossing the ring (i.e. from odd to even or vice versa) so as to be the same as that of the outgoing wave, which opens the transmission. This phenomenon is further illustrated by the LDOS of figure 3. In the energy regime (II) of figure 2, i.e. the case of different parity, the spatial variation of LDOS (e.g. at $E = 0$) along the transport direction is strong at $B = 0$ and the transmission is blocked, while it becomes invisible at $B = 0.5 \times \phi_0/S$, so that the structure is very transparent. Conversely, in the regimes (I) and (III), i.e. the case of same parity, this variation (e.g. at $E = 120$ meV) is invisible at $B = 0$ but strong at $B = 0.5 \times \phi_0/S$. Thus, the picture of phase shifts above explains well the transport phenomena observed.

The difference between the results displayed in figures 2(*b*) and (*c*) can be understood as follows. If Q_r is even, the parity selective rule applies to the transmission along the ring arms, so that a clear energy gap is still observed. However, this effect of parity selective rule weakens and the transparence becomes high at the energy points close to the potential energy of the *n*−doped or p-doped zone because, in these cases, the charge carriers along the ring arms are almost in one type of band, i.e. in the first valence or conduction subband, respectively. This effect also vanishes if Q_r is odd; or, for even Q_r, if the ring is totally located in the zone of a unique doping type. The ring can hence be transparent in almost the whole gap region when applying a finite B−field.

The transport properties observed are expected to govern interesting electrical behaviors of the ring. We display the current and corresponding MR as a function of bias voltage in figure 4(*a*) and B−field in figures 4(*b*) and (*c*). At $B = 0$, the current is small at low bias due to the presence of the energy gap (II). When raising the bias, this gap reduces and hence the current increases. At high bias, when the potential profile ($U_R = U_0 - eV_b$) in the p-doped region moves down to come

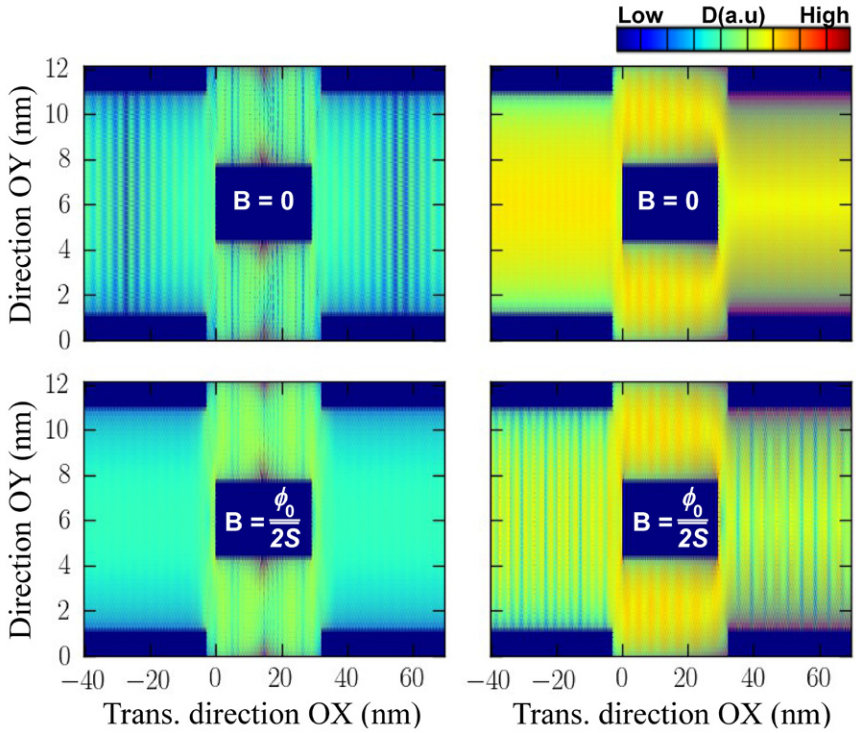

Figure 3. Local density of states plotted at $E = 0$ (left panels) and 120 meV (right panels) for two different B−fields in the ring studied in figure 2(*c*).

below that in the n-doped zone, this energy gap re-increases and the current reaches a saturation regime. Obviously, when varying the B−field, the current exhibits strong AB oscillations with a π−phase difference between low and high biases. Note that in the former case, the transmission in the energy regime (II) is dominant while in the latter one the regimes (I) and (III) govern the conduction. Accordingly, we observe (i) a giant positive (negative) MR at low (high) bias and (ii) a strong NDC behavior at $B = (n + ½)\,\phi_0 / S$, e.g. $B = 0.5 \times \phi_0/S$ here. In particular, a giant positive MR of about 95% at low bias, a giant negative MR (with a peak at $V_b = U_0/e$) of thousands % at high bias and the NDC behavior with a high peak-to-valley ratio (PVR) of about 28 are observed.

Interestingly, the rings studied here provide not only strong MR and NDC effects but also various possibilities to control these effects. In particular, we can modulate periodically the MR by tuning the B−field and can switch this quantity from a positive to a negative value by varying the bias. Similarly, the NDC behavior and the form of I–V characteristics can also be modulated periodically by varying the B−field. The controllability of NDC behavior has also been observed by tuning the gate voltage in tunnel field-effect transistors (see [24] and references therein) and is suitable for designing circuits operating at high frequency [25]. It is important to keep in mind that the NDC behavior observed here has a different origin from the similar effects previously explored in the literature, i.e. the peak (valley) current is governed by the AB interference within the transmission between two states of different (same) parity.

We now would like to discuss the dependence of the MR and NDC effects on the structure parameters. Since the transport in the ring essentially depends on the balance between the contributions of the energy regimes (I–III) indicated in figure 2 (i.e. depends on U_0 and the band structure of contact GNRs), we display in figure 5 the I–V characteristics and magnetoresistance at $B = 0.5 \times \phi_0/S$ obtained in the ring of narrower contact GNRs $Q_c = 30$ with different potential barriers U_0. Actually, the width of contact GNRs plays an important role since it determines the energy range of single band transport (i.e. energy regimes (I–III)), in which the strong AB oscillations are achieved. Due to confinement effects, this energy range ($E_{sb} \equiv 2\Delta$ with Δ determined in figure 1) is dependent on the GNR width according to the scaling rule $E_{sb} \propto 1/Q_c$. In particular, E_{sb} takes the values of about 0.80, 0.53 and 0.40 eV for $Q_c = 30$, 46 and 62, respectively. Due to this scaling rule, a change in the width of contact GNRs has a significant influence on the current at high bias. In particular, the MR peak at $V_b = 0.2$ V ($\equiv U_0/e$) takes the values of about -2.4×10^4%, -1.0×10^4% and -2.1×10^3% for the three cases of Q_c above, respectively, while the results obtained at low bias are weakly affected. Additionally, we also find that NDC behavior at $B = 0.5 \times \phi_0/S$ is stronger when reducing Q_c, i.e. the PVR is about 62 for $Q_c = 30$ while it is only about 28 for $Q_c = 46$. Thus, these results suggest that to observe the strong effects described above, the narrow contact GNRs (i.e. smaller than about 10 nm or $Q_c \lesssim 46$) should be used. In figure 5, when increasing U_0, though the negative MR peak and the PVR are slightly reduced, we find that, because the energy regime (II) is enlarged, (i) the current peak of NDC behavior at $B = 0.5 \times \phi_0/S$ increases significantly; (ii) the positive MR can approach almost 100% ; (iii) the bias windows of the giant positive and giant negative (i.e. $>10^3$%) MR are both

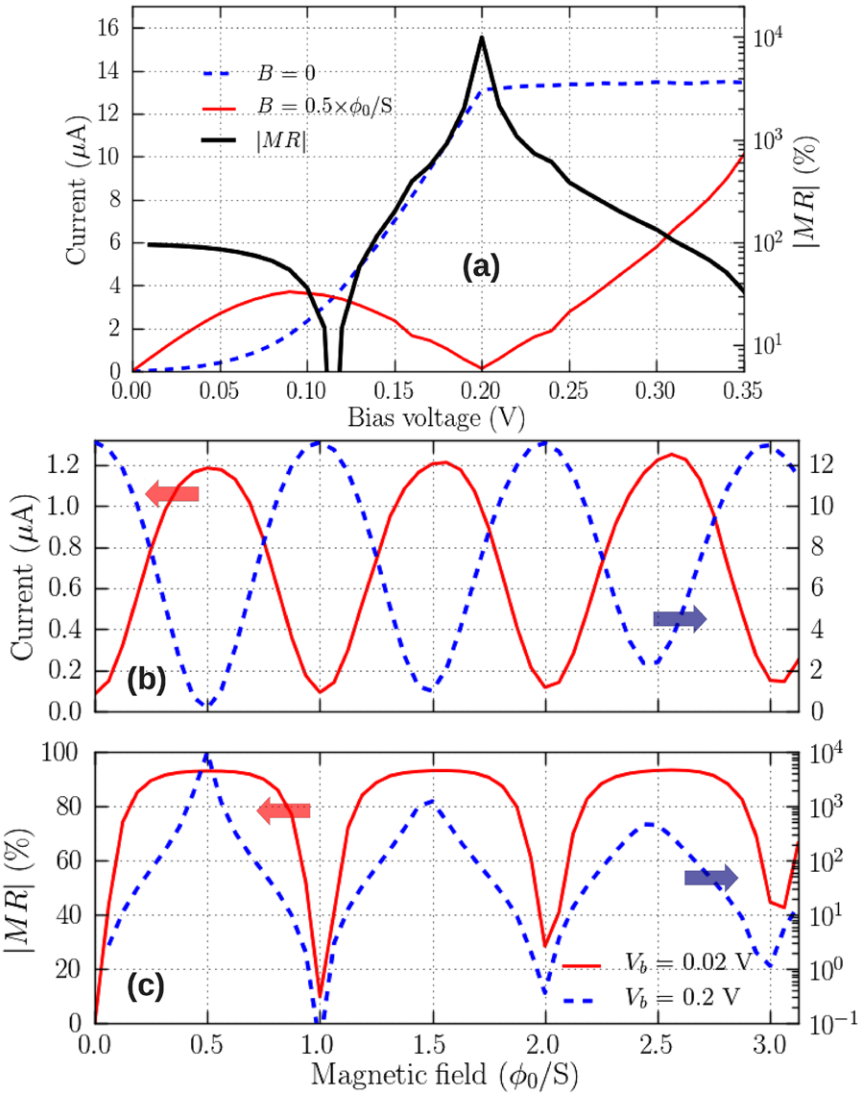

Figure 4. (*a*) *I*–*V* characteristics (see the left axis) of the GNR ring studied in figure 2(*c*) at $B = 0$ and $0.5 \times \phi_0/S$ and its corresponding MR (see the right axis). (*b*) Current and (*c*) MR as a function of B–field at different biases. All calculations were performed at room temperature.

enlarged. These properties are well pronounced in the range of $U_0 \lesssim 2\Delta$. Beyond this range of U_0, the transport picture can be disturbed by the contribution of high-energy subbands, which has been shown to weaken the AB interference [19].

As discussed above, since it is a key parameter for the AB oscillations, the scaling rule with respect to the ring size (length and width) should also be clarified (see also the discussion in [19]). An increase of the ring length makes the ring area S larger, which simply modulates the period of AB oscillations and offers the possibility of high MR at low magnetic field. In addition to this effect, an increase of the ring width also increases the size of side nanoribbons, whose armchair edges are different from the zigzag edges of the top and bottom GNR arms. This can enhance the inhomogeneity of transport trajectories along the ring arms. For a too large Q_h/Q_c ratio, this inhomogeneity can prevent the AB interference from taking place properly. In this case, only the resonant tunneling effect due to the ring geometry is significantly pronounced, as reported for similar structures in [26–28]. Therefore, a small Q_h/Q_c ratio is mandatory to guarantee strong AB interference and the MR effect.

Regarding the graphene *pn* junctions, in addition to the transport properties reported here, it has been recently shown that the occurrence of snake states in the *pn* interface is another fascinating feature [29–32]. They can play an important role in the charge transport, especially in the multi-terminal *pn* junctions where the transport takes place along the junction interface. In particular, it was demonstrated in [29] that the effects of snake states reduce the resistance along the interface, while the resistance across the interface increases. In [30], unusual properties of Hall resistance and band resistance were observed in the Hall bar structures based on a graphene *pn* junction under a magnetic field. The current oscillations due to the snake states with respect to the geometric structures were observed in [32]. Indeed, these snake states also occur in the rings we have considered, resulting in localized states in the GNR edges at the *pn* interface as shown in the LDOS at $x \simeq 15$ nm in the left panels of figure 3. However, our calculations do not show any

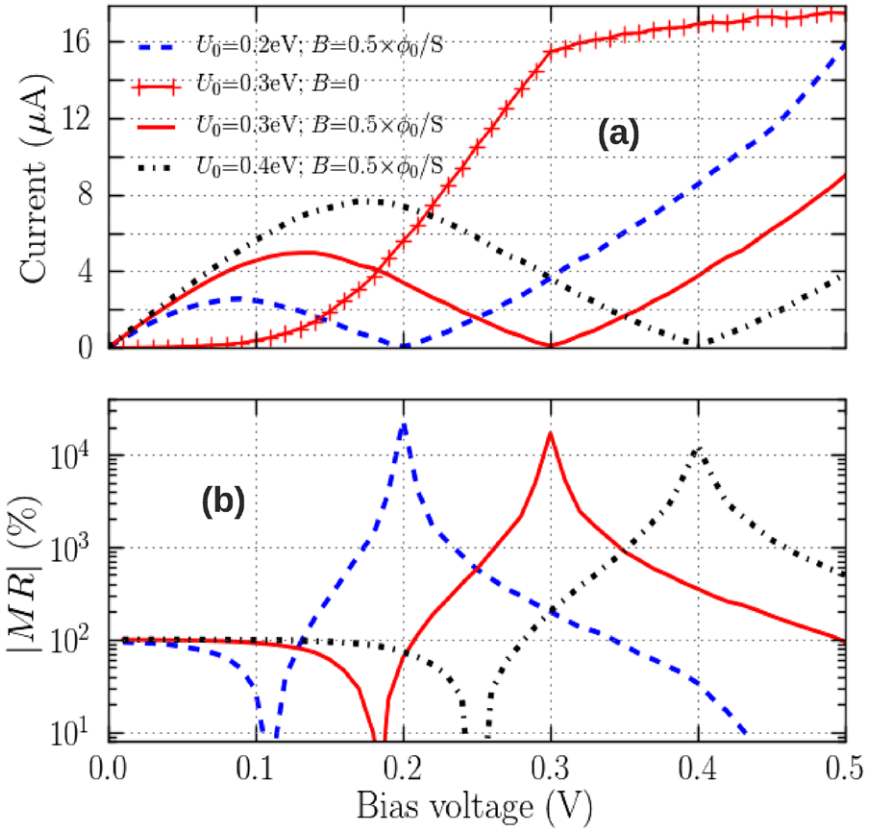

Figure 5. (*a*) Current and (*b*) corresponding MR at $B = 0.5 \times \phi_0/S$ as a function of bias voltage in the GNR ring of $Q_c = 30$ with different U_0. Other parameters are the same as in the ring studied in figure 2(*c*). All calculations were performed at room temperature.

significant effect of these states on the transport through the ring. This may be understood by the fact that differently from the multi-terminal graphene *pn* junctions mentioned above, in our two-terminal systems the transport direction is definitely perpendicular to the junction interface. Hence, the snake states cannot play any important role in the transport, while the effects of the parity symmetry of wave functions are dominant.

We would like to mention that several experiments (e.g. [12, 13, 23, 33] and see also the review [7]) have demonstrated clear *h*/*e*—AB oscillations in graphene rings. However, in these works the authors have not observed an AB effect as strong as we obtained here. There may be two main reasons for this [19]. On the one hand, in the graphene rings previously studied, the contact GNRs are too large, making it difficult to observe the strong AB effect related to the single band energy regime. On the other hand, compared to our rectangular rings, these rings have a circular shape and irregular GNR edges along the arms. This makes the trajectories of charge carriers along the ring arms strongly inhomogeneous and hence the AB effect cannot take place properly. Therefore, to achieve a strong AB effect, our study suggests using ring geometries with narrow (i.e. $\lesssim$10 nm as discussed above) contact GNRs and with homogeneous ring arms, as in the rectangular rings shown here. In addition, the good control of ribbon edges is another important issue. However, our calculations show that the strong AB effects can still be achieved in the cases when the edge disorder is not too strong, i.e. the disorder probabilities $P_D < 10\%$ as in [19]. Moreover, besides the top-down techniques successfully used to fabricate narrow GNRs at the nanometer scale, ultra-narrow GNR systems have been recently realized using surface-assisted bottom-up techniques [34–37] with atomically precise control of their topology and width. These techniques not only allow for the fabrication of ultra-narrow GNRs but also give access to GNR heterostructures [37]. Based on this, one can optimistically expect that the fabrication of the considered rings without or with a weak disorder may be achieved soon, which would allow experimental verification of our predictions.

Finally, we would like to make one more remark regarding the nearest-neighbor tight binding model used in this work. To compute more accurately the electronic transport in graphene nanostructures, farther-neighbor interactions might need to be considered. However, our calculations here are still reasonable for the following reasons. On the one hand, as discussed in [17], the longer range interactions do not have any influence on the parity symmetry of wave functions because this symmetry is essentially controlled by the space mirror symmetry of the crystal Hamiltonian. On the other hand, the higher order neighbor interactions result mainly in changes in high energy bands [38] while in this work we focus on the regime of single band transport (i.e. at low energy). Therefore, taking into account the higher order neighbor interactions as in [38] should result in only a slight change in our results at high bias.

In summary, we have investigated the interplay between the AB interference and parity selective tunneling in *pn* junctions based on zigzag GNR rings, where the contact GNRs have an

even number of zigzag lines. We find that the AB interference can reverse the parity symmetry of incoming waves, so that the transmission between two states of different parity, which is blocked at $B = 0$, can be opened when applying a finite B−field. As an important result, the AB oscillations of these transmission processes exhibit a π−phase shift, compared with the case of states of same parity. On this basis, interesting effects such as giant (both positive and negative) MR and strong NDC behavior can be achieved at room temperature. The study also suggests possibilities to control/improve these effects by tuning the applied voltage, the B−field and the doping profile.

Acknowledgments

This research in Hanoi is funded by Vietnam's National Foundation for Science and Technology Development (NAFOSTED) under grant no. 103.02-2012.42. PD acknowledges the French ANR for financial support under the projects NANOSIM-GRAPHENE (grant no. ANR-09-NANO-016) and MIGRAQUEL (grant no. ANR-10-BLAN-0304).

References

[1] Aharonov Y, Bohm D 1959 *Phys. Rev.* **115** 485
Peshkin M and Tonomura A 1989 *The Aharonov–Bohm Effect Lecture Notes in Physics* vol 340 (Heidelberg: Springer)
[2] Webb R A, Washburn S, Umbach C P and Laibowitz R B 1985 *Phys. Rev. Lett.* **54** 2696
[3] Datta S, Melloch M R, Bandyopadhyay S, Noren R, Vaziri M, Miller M and Reifenberger R 1985 *Phys. Rev. Lett.* **55** 2344
[4] Bachtold A, Strunk C, Salvetat J-P, Bonard J-M, Forro L, Nussbaumer T and Schonenberger C 1999 *Nature* **397** 673
[5] Lassagne B, Cleuziou J-P, Nanot S, Escoffier W, Avriller R, Roche S, Forro L, Raquet B and Broto J-M 2007 *Phys. Rev. Lett.* **98** 176802
[6] Peng H, Lai K, Kong D, Meister S, Chen Y, Qi X-L, Zhang S-C, Shen Z-X and Cui Y 2010 *Nature Mater.* **9** 225
[7] Schelter J, Recher P and Trauzettel B 2012 *Solid State Commun.* **152** 1411
[8] Castro Neto A H, Guinea F, Peres N M R, Novoselov K S and Geim A K 2009 *Rev. Mod. Phys.* **81** 109
[9] Katsnelson M I, Novoselov K S and Geim A K 2006 *Nature Phys.* **2** 620
[10] Nam Do V, Hung Nguyen V, Dollfus P and Bournel A 2008 *J. Appl. Phys.* **104** 063708
[11] Schelter J, Bohr D and Trauzettel B 2010 *Phys. Rev.* B **81** 195441
[12] Smirnov D, Schmidt H and Haug R J 2012 *Appl. Phys. Lett.* **100** 203114
[13] Rahman A, Guikema J W, Lee S H and Markovic N 2013 *Phys. Rev.* B **87** 081401
[14] Wang Z F, Li Q, Shi Q W, Wang X, Yang J, Hou J G and Chen J 2008 *Appl. Phys. Lett.* **92** 133114
[15] Rycerz A, Bardarson J H, Rycerz A and Beenakker C W J 2007 *Nature Phys.* **3** 172
[16] Akhmerov A R, Bardarson J H, Rycerz A and Beenakker C W J 2008 *Phys. Rev.* B **77** 205416
[17] Cresti A, Grosso G and Parravicini G P 2008 *Phys. Rev.* B **77** 233402
[18] Nakabayashi J, Yamamoto D and Kurihara S 2009 *Phys. Rev. Lett.* **102** 066803
[19] Hung Nguyen V, Niquet Y M and Dollfus P 2013 *Phys. Rev.* B **88** 035408
[20] Hung Nguyen V, Saint-Martin J, Querlioz D, Mazzamuto F, Bournel A, Niquet Y-M and Dollfus P 2013 *Comput. Electron.* **12** 85
[21] Peierls R E 1933 *Z. Phys.* **80** 763
[22] Schelter J, Trauzettel B and Recher P 2012 *Phys. Rev. Lett.* **108** 106603
[23] Huefner M, Molitor F, Jacobsen A, Pioda A, Stampfer C, Ensslin K and Ihn T 2010 *New J. Phys.* **12** 043054
[24] Hung Nguyen V, Niquet Y M and Dollfus P 2012 *Semicond. Sci. Technol.* **27** 105018
[25] Mizuta H and Tanoue T 1995 *The Physics and Applications of Resonant Tunneling Diodes* (Cambridge: Cambridge University Press)
[26] Zhang Z Z, Wu Z H, Chang K and Peeters F M 2009 *Nanotechnology* **20** 415203
[27] Wu Z, Zhang Z Z, Chang K and Peeters F M 2010 *Nanotechnology* **21** 185201
[28] Munarriz J, Dominguez-Adame F and Malyshev A V 2011 *Nanotechnology* **22** 365201
[29] Williams J R and Marcus C M 2011 *Phys. Rev. Lett.* **107** 046602
[30] Barbier M, Papp G and Peeters F M 2012 *Appl. Phys. Lett.* **100** 163121
[31] Zarenia M, Pereira J M Jr , Peeters F M and Farias G A 2013 *Phys. Rev.* B **87** 035426
[32] Chen J-C, Xie X C and Sun Q-F 2012 *Phys. Rev.* B **86** 035429
[33] Russo S, Oostinga J B, Wehenkel D, Heersche H B, Sobhani S S, Vandersypen L M K and Morpurgo A F 2008 *Phys. Rev.* B **77** 085413
[34] Cai J *et al* 2010 *Nature* **466** 470
[35] Huang H, Wei D, Sun J, Wong S L, Feng P F, Castro Neto A H and Wee A T S 2012 *Sci. Rep.* **2** 983
[36] Ruffieux P *et al* 2012 *ACS Nano* **6** 6930
[37] Blankenburg S, Cai J, Ruffieux P, Jaafar R, Passerone D, Feng X, Mullen K, Fasel R and Pignedoli C A 2012 *ACS Nano* **6** 2020
[38] Reich S, Maultzsch J, Thomsen C and Ordejón P 2002 *Phys. Rev.* B **66** 035412